NTNU

Norwegian University of
Science and Technology

Optimizing carbon coating of silica from diatom frustules as a high performance, low cost and environmentally friendly anode material for lithium ion batteries

Sigrun Sofie Berg

Nanotechnology
Submission date: October 2018
Supervisor: Fride Vullum, IMA

Norwegian University of Science and Technology
Department of Materials Science and Engineering

Preface

Most experiments and analysis described in this work was carried out by the author, with the exception of surface area measurements of silica from diatoms and milled silica from diatoms done by researcher Andreas N. Norberg.

I would like to thank my supervisor, Fride Vullum-Bruer, for guidance, motivation and encouragement. Co-supervisor Andreas N. Norberg also deserves my gratitude for helping me when I needed it the most, both in the lab and as emotional support, and for always being available and motivated when I went by his office.

Sigrun Sofie Berg
21.10.2018, Trondheim

Abstract

The goal of this work was to optimize the carbon coating of silica from diatom frustules as a high performance, low cost and environmentally friendly anode material for lithium ion batteries. This was done by investigating the influence of carbon coating with sucrose as the carbon precursor. The diatoms were washed, calcined and milled before carbon coating by mixing with sucrose and finally pyrolysed.

To optimize the carbon coating of silica, the sucrose and silica mix was pyrolysed between 650°C and 1050°C. After choosing an ideal temperature of 1050 °C due to decreased surface area and increased I_D/I_G ratio, the influence of carbon content was investigated by electrochemical characterization.

Galvanostatic cycling revealed that the capacity of the pure silica cell dropped significantly with carbon coating. The pure silica cell displayed a capacity of 790 mAh/g after 50 cycles compared to 386 mAh/g after 50 cycles for the silica cell with 4.8 wt% carbon coating. The capacity decreased further with increasing carbon content, suggesting that the carbon coating hampers the silica conversion of the cells. This was confirmed by the potential profiles of the cells showing an increase in solid electrolyte interface formation, and decrease in silica conversion as the carbon content increased. From this it can be concluded that a carbon content of 4.8% and above inhibits silica conversion at the specific current utilized in this work.

Sammendrag

Silika utvunnet fra diatomer har et potensiale som billige og miljøvennlige anoder med høy ytelse til bruk i litiumionebatterier. Målet med denne oppgaven var å forbedre disse anodene ved å dekke dem med karbon derivert fra sukrose. Først ble diatomene vasket og kalsinert før de ble blandet med sukrose og pyrolysert. Karbonlaget ble optimert ved å pyrolysere en blanding av sukrose og silika mellom 650°C og 1050 °C. På grunn av lavere overflateareal og høyt I_D/I_G forhold ble 1050 °C valgt som pyrolysetemperatur på de produserte anodene. Disse ble laget med forskjelligt karboninnhold og undersøkt ved elektrokjemisk karakterisering.

Galvanostatisk sykling viste at karbondekket senket ladningskapasiteten til anodene fra 790 mAh/g etter 50 sykluser for en ren silikaanode til 386 mAh/g etter 50 sykluser for anoden med 4.8 vekt% karbondekke. At ladningskapasiteten synker med økende karboninnhold tyder på at karboninnholdet hindrer silikakonvertering i anoden. Dette ble bekreftet av potensialprofilene til de forkjellige cellene som viste økt solid elektrolyttgrensesnittformasjon og senket silikakonvertering ved økt karboninnhold. Fra dette kan man konkludere at et karboninnhold på 4.8 % eller mer, hindrer silikakonvertering i anoden ved strømtettheten brukt i denne oppgaven.

Contents

Introduction

The contribution of carbon dioxide to the greenhouse effect was first evaluated by Arrhenius in 1896 [1]. Since then, the amount of carbon dioxide in the atmosphere has increased drastically due to the burning of fossil fuels. This has been calculated to have increased the global surface temperature by 0.6 °C during the 20th century [2] . Global warming has already had a negative impact on plant and animal populations [3], sea levels and weather patterns [2]. To decrease – and hopefully reverse – some of the negative impact of global warming, a big effort is required to decrease the need for fossil based energy. Transforming to solar, wind and other forms of renewable energy sources is a necessity. The drawbacks of solar, wind and other weather dependent renewable energy sources are the expense per watt hour of energy produced and the weather dependency of the technology. Solar power is getting more efficient, but production is still highest at midday. When added to the electrical grid, a massive surge in electricity demand after sunset puts a high strain on the power system [4]. Wind energy is also getting cheaper as more efficient wind turbine transformers are developed [5] .

This increase in energy storage demand from renewable energy sources creates a need for better batteries. Additionally, electrical vehicles are also necessary to decrease fossil fuel consumption, which also require better batteries to improve their range. To be able to make this change, improvements are required both in terms of capacity, power density, energy density and sustainability of the batteries. Due to their low weight, lithium ion batteries (LIB) have sufficient energy density to run electrical vehicles. The technology was commercialized by Sony in 1992 [6], and accounted for a 80 % market share of rechargeable batteries by 2007 [7]. The environmental impact of LIBs is lower than that of lead acid batteries [8], and electrical vehicles run by LIBs have less of av environmental impact compared to conventional vehicles [9] . However, this is highly dependent on the electricity source utilized to run the electrical vehicle. The production of LIBs is dependent on the production of lithium metal, which is a finite source. The lithium sources on earth will most likely not be depleted during the next century [10], though the price will rise as the demand increases. The global warming potential of LIBs is increased by the use of the solvent N-methyl-2-pyrrolidone (NMP) in graphite and electrode production [11]. Replacing NMP with water as an electrode solvent can decrease CO_2 emissions from the battery production by 22.7 % [11]. However, electricity storage for windmills and photovoltaic cells connected to the electricity grid, requires a significant increase in the energy and power density of the batteries used today. One solution to this is to increase the capacity of the anode as the currently used anodes are made from graphite with a theoretical potential of 372 mAh/g [12] .

Silica anodes for LIB have a theoretical capacity of between 749 mAh/g [13] and 1965 mAh/g [14], and have displayed capacities around 1400 mAh/g at 1 A/g for 200 cycles [15] . Silica is abundant – as the earths crust consists of 59% silica [16] –, has no major safety concerns, and is already widely utilized in glass and electronic industries. Due to the small

volume expansion during insertion and extraction of lithium ions, the anode has great cycling stability. Note that only nanosized amorphous silica reacts with lithium [17].

Amourphous nanostructured silica can be obtained by high energy milling [18], or by calcination of diatoms [19]. Diatoms contain a silica cell wall called a frustule, which has a surface patterning of porous silica on a meso and nano scale [20] . Diatoms present a cheap, environmentally friendly and easily accessible precursor for the production of solar cells, gas sensors, electroluminecent devices and battery anodes [21]. As diatoms are a substantial part of the marine ecosystem [22], they can easily be harvested. The porosity and surface structure of the silica frustule is beneficial for an anode material, resulting in easier penetration of lithium ions.

Silica is not electrically conducting, which is required by an electrode to be able to transfer electrons to the current collector. Improving the conduction of silica electrodes has been achieved by mixing with carbon [18], composites with silicon and carbon [23] and carbon coating [14, 24, 25, 26].

The reported specific capacities for silica anodes produced from diatoms are 500 mAh/g at 18mA/g over 50 cycles [19] , 600 mA/h at 50mA/g over 100 cycles [27] and 200 mAh/g at 200 mA/g over 100 cycles [28].

Aim of work

The goal of this work is to optimize the carbon coating of silica from diatom frustules as a high performance, low cost and environmentally friendly anode material for lithium ion batteries. This was done by investigating the influence of carbon coating with sucrose as the carbon precursor. First, the optimal pyrolysis temperature for carbon coating silica was found. Second, active material with varying carbon content was produced and subjected to electrochemical characterization.

1. Theory

1.1 Electrochemical cells and secondary batteries

The history of the modern battery started with Alessandro Volta's cell in 1782 [29], and has now become a staple of modern society. Energy storage and production are changing in society as sustainable energy sources are getting more effective and cheaper [30].

Electrochemical cells are defined by chemical energy converting into electrical energy. Batteries are a type of electrochemical cell, and are divided into primary and secondary cells. Primary cells were the first ones that were made and they are defined by their irreversible nature. They transform chemical energy into electric energy irreversibly and can not be recharged. Secondary cells are based on reversible reactions, implying that the reactions can be reversed by supplying electrical energy [12].

Both primary and secondary batteries consist of five main components. Two electrodes connected to current collectors, an electrolyte and a separator. The most basic set up is shown in Figure 1.2, where the electrodes are connected by an electrically conductive wire and an ionic solution (the electrolyte). The reaction is driven by the potential difference, U, between the electrodes and results in an electric current.

In an electrochemical cell there will be one half cell reaction on each electrode. The reaction on the anode releases electrons and is an oxidation reaction, and the reaction on the cathode consumes electrons and is a reduction reaction. In a secondary battery this is correct during discharge, and will change during charge. Therefore the definition of the cathode in a secondary battery is the electrode with the highest potential, and the anode is the electrode with the lower potential. This makes the cathode the positive electrode and the anode the negative electrode. In all electrochemical cells the electrons travel between the electrodes through the circuit, and to maintain a charge equilibrium the electrolyte conducts ions between the electrodes.

The potential difference, ΔU, between the electrodes can be found using the difference in Nernst potential between them. Taking a generalized half cell reaction:

$$\mathrm{v_A A} + \mathrm{v_B B} + \mathrm{ne^-} \longrightarrow \mathrm{v_C C} + \mathrm{v_D D} \tag{1.1}$$

where A and B are the reactants, and C and D are the products. v_x are integers describing the amount of molecules involved in the reaction, e^- are electrons and n is the number of electrons.

The Nernst potential can be derived from the Gibbs free energy [31], and gives:

$$\mathrm{E}=\mathrm{E_0} + \frac{\mathrm{RT}}{\mathrm{nF}} \ln \frac{(\mathrm{a_C})^{\mathrm{v_C}} (\mathrm{a_D})^{\mathrm{v_D}}}{(\mathrm{a_A})^{\mathrm{v_A}} (\mathrm{a_B})^{\mathrm{v_B}}} \tag{1.2}$$

where R is the universal gas constant, T is the temperature, n is the number of electrons involved in the half cell reaction, F is the Faraday constant, and a is the chemical activity of the constituents of the half cell reaction.

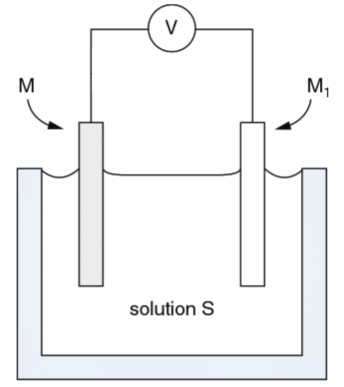

Figure 1.1: Electrochemical cell where M and M_1 are the electrodes, S is the electrolyte and V is the potential difference between the electrodes. Adapted from Lithium Batteries by Scrosati [31].

This electrochemical cell can be made in many forms that are more portable than in Figure 1.2, and the electrodes and the electrolyte can be made from either solid, liquid or soft materials. The most common set up is with liquid electrolyte and solid electrodes, however, solid electrolytes are heavily researched [12].

1.1.1 Lithium batteries

Lithium ion batteries are now the primary energy storage devices used in society [7]. They are in everything from personal electronics to electric vehicles, and to integrate windmills and photovoltaic plants onto smart grids [12, chapter 10].

Lithium batteries can be separated into lithium ion batteries (LIB) and lithium metal batteries (LMB). The difference between the two is that LMBs use lithium metal as a lithium source whereas LIBs use intercalation compounds. Because of dendrite formation during cycling in LMBs they are often used in primary batteries and most secondary lithium batteries are LIBs. Dendrites occur when lithium ions are deposited on lithium metal, and instead of depositing in an even layer the ions nucleate on the nearest lithium metal surface. This creates lithium structures growing out of the electrode surface and can cause short circuits in the battery. The typical gravimetric densities are 250 Wh/kg for LMBs and 150 Wh/kg for LIBs [12].

The attractiveness of lithium for battery use is the high specific capacity of 3860 mAh/g and its high standard redox potential of -3.04 V against H_2/H^+ . Lithium is a light metal (0.51 g cm^{-3}) with the electric configuration of (He)$2s^1$. Consequently it has both a high potential for battery use and is highly reactive. In its pure form it has a high reactivity with air, nitrogen and water [12]. The reactivity of lithium makes it hard to work with. That is why it took five decades from G. N. Lewis began researching the potential of lithium batteries in 1912 [32] to the breakthrough by Harris in 1958 [33]. Harris discovered the stability of lithium in various non-aqueous electrolytes which marked the beginning of the commercialization of primary lithium cells. Rechargeable cells took longer time to produce as lithium metal electrodes form dendrites with cycling.

In the late 1970s the idea of intercalation compounds as electrodes was suggested to improve secondary lithium cells. Intercalation compounds are layered host materials in which ions can move around easily. The research of Goodenough et. al. on $LixCoO_2$ [34, 35] led to the first commercialized LIB by Sony in 1992 [6].

1.1.2 Battery terminology

The energy storage capability of batteries can be expressed in different ways. Both volumetric energy density (Wh/cm^3) and gravimetric energy density (Wh/kg) is used. When producing an electric car there are both volume and mass limits, so both of these would be important. Energy stored in a battery is given by:

$$E = \int_0^{\Delta t} I \cdot V(t)\delta t = \int_0^{Q} V(q)dq \tag{1.3}$$

where E is energy, I is current, V is voltage, t is time, Q is the total charge per unit weight and q is the state of charge.

As seen in Equation (1.3) specific capacity (mAh/g), Q, is closely related to the energy of a battery and is therefore a useful term. Capacity describes how much charge is stored in the electrode. As batteries operate on different voltages due to the materials used, capacity make them easier to compare. However, the voltage range of the battery determines the energy stored by the charge as described by Equation (1.3). Charge capacity is the charge stored in the battery and discharge capacity is the charge drawn from the battery [36].

When describing the functionality of a battery the efficiency change between each charge and discharge cycle is important to predict how the battery will work after time. Coulombic efficiency is given by:

$$\text{Coulombic efficiency} = \frac{\text{charge capacity}}{\text{discharge capacity}} \cdot 100\% \tag{1.4}$$

and describes how much of the charge input that is obtainable as an output. High coulombic efficiency indicates a highly reversible cell, while low coulombic efficiency indicates capacity losses due to irreversible reactions of the cell.

Polarization

Polarization, or overvoltage, in a battery is an internal resistance decreasing the output voltage, V_{dis}, and increasing the input voltage, V_{ch}, from the open circuit voltage, V_{oc}. This internal resistance is denoted η, and is dependent on the state of charge (SOC) and the current [36]. Described by the following equations [36]:

$$V_{dis} = V_{oc} - \eta(SOC, I_{dis}) \tag{1.5}$$

$$V_{ch} = V_{oc} + \eta(SOC, I_{ch}) \tag{1.6}$$

Polarization occurs due to ohmic, kinetic and transportation overvoltage. Ohmic polarization, η_{ohm}, manifests as a resistance due to slow ionic migration, and is defined as $\eta_{ohm} = IR$. Where I is the electric current and R is the internal battery resistance. Because of this the ohmic polarization of an electrode is often called IR loss or IR drop. Kinetic polarization occurs due to slow rate kinetics of electrode reactions and transportation polarization occurs when supply of reactants or removal of products is the cause of slow reactions. The capacity of a battery can vary with the current applied due to polarization of the electrode [37].

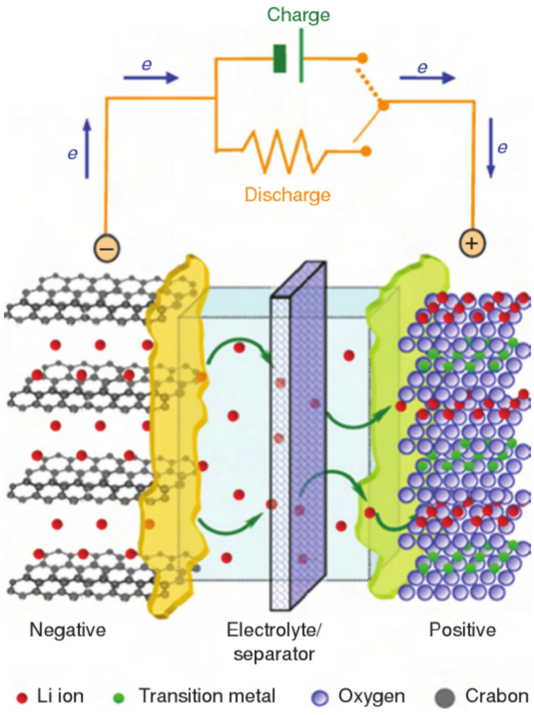

Figure 1.2: A generalized lithium battery and its components. In this representation the negative anode consists of graphite and the positive anode consists of a transition metal oxide. The figure is showing the discharge of the battery as lithium ions are extracted from the anode, pass through the electrolyte and separator and are inserted into the cathode. The electron flow is also displayed from the current collector on the anode to the current collector on the cathode. Adapted from Lithium batteries by Scrosati [31].

1.2 Cell components

In this section the anode, electrolyte and binder will be further described for batteries in general and for LIBs in particular. Cathode, separator and current collector will be briefly described as well. A generalized LIB can be seen in Figure 1.2. A conventional LIB has a negative graphite electrode, and a positive transition metal oxide electrode (typically $LiCoO_2$). The electrolyte consists of $LiPF_6$ in carbonate solvent with a separator in the middle to prevent electrical contact between the electrodes, while facilitating ion flow. Current collectors are used to improve the electron flow to and from the electrodes, thus improving the reaction kinetics.

1.2.1 Anode

The first commercial LIB made by Sony in 1992 had graphite as the active element of the negative electrode. Graphite is still the most common material used, but other materials such as silicon, titanium oxide and silica are potential new anode materials.

There are six requirements an ideal anode should fulfill[12]:

1. It has to be light and able to accommodate as much Li as possible to obtain a high gravimetric energy density.

2. The redox potential against Li_0/Li^+ has to be as small as possible at any Li concentration. This is because the difference in redox potential gives the overall voltage of the cell.

3. High ionic and electronic conductivity to facilitate high mobility of the Li ions. High mobility increases the power density and rate capability of the cell.

4. It must not be soluble in the electrolyte or react with the lithium salt so it will not disintegrate with cycling.

5. It must be safe to use, and not produce dangerous amounts of heat with cycling.

6. Should be cheap and environmentally friendly.

The reversible intercalation of lithium ions in graphite results in LiC_6. Increasing the lithium content is possible, but is not reversible. The conversion of C to LiC_6 gives a theoretical capacity of 372 mAh/g. One of the main reasons to look for other types of anode materials is to increase the capacity of LIB. Production of graphite anodes also uses the solvent N-Methyl-2-pyrrolidone (NMP) which is harmful to the environment and requires many safety procedures [38].

During the last century a lot of anode materials have been researched for use in LIBs, ranging from metals to intermetals and oxides [12]. However, in resent years there has been a greater focus on the materials listed in Table 1.1.

Table 1.1: Theoretical capacities of anode materials for LIBs [12].

Anode material	Theoretical capacity [mAh/g]
Graphite	372
Silicon	4200
Germanium [39]	1624
Tin	960
Titanium dioxide	335
$Li_4Ti_5O_{12}$	175
Silicon dioxide [13, 14]	749-1965

Carbon conductive additives

As previously mentioned, the ionic and electronic conductivity of an anode are very important. Therefore, anode materials with low conductivities are often mixed with more conducting materials to improve performance. Carbon additives, such as carbon black and acetylene black, are often used because of their great conductivity and their known compatibility with lithium. Their role in the anode is to facilitate electron conduction from active material to current collector [40], and several examples of this can be found in literature [41, 15, 42].

The porosity of carbon enhances the absorption of electrolyte into the electrode. This ensures good contact between the active material, the electrolyte and the current collector. Good contact is preferable both for the electronic and ionic conduction in the electrode. However, if too much carbon is added the increased viscosity of the electrode decreases the ionic conductivity [40].

Binder

When an electrode consists of an active material mixed with e.g. a carbon filler, a binder ensures the mechanical stability of the electrode, and secures the adhesion both between electrode particles and between the particles and the current collector. The binder is usually a polymer compound and because it is insulating and electrochemically inactive, the amount added to the electrodes should be minimized [40].

Traditionally, binder properties have been overlooked when it comes to battery performance. However, they can have a great impact on the stability and irreversible capacity losses of the battery. Recently there have been several improvements on the stability of LIBs with binders such as polyacrylic acid and styrene-butadiene copolymer [40, 43].

Alginate, a natural polysaccharide from brown algae, has been compared to the common LIB binder polyvinylidene difluoride (PVDF). When immersed into electrolyte solvent the alginate binder retained the same stiffness, and did not show detectable swelling. PVDF on the other hand became almost 50 times softer and showed a swelling of ~ 20 % of the thickness. The alginate binder proves a low polymer/electrolyte interaction, and is expected to decrease unwanted deterioration of silicon anodes [44].

1.2.2 Electrolyte

The primary role of the electrolyte is to conduct ions between the electrodes. To be able to do this, it has to have an optimal electrode-electrolyte interface chemistry for both electrodes. The electrodes will dictate which electrolyte is chosen, but there are several other criteria that should be met to make the battery practical, safe and stable. The phase stability is important, as it is problematic if the electrolyte crystallizes or vaporizes. It should also be non-flammable, have a wide elecrochemical stability window and be robust against mechanical and thermal conditions to ensure the battery's safety. To ensure low cost and limit the environmental impact, the material should be abundant, non-toxic and envirnomentaly friendly. To ensure good performance the electrolyte should have good wetting properties at both electrodes, and be non-corrosive to battery components. An ideal electrolyte is hard to find, but it is important to take all these criteria under consideration [12].

In current commercial LIBs aprotic organic solvents such as ethylene carbonate or dimethyl carbonate are commonly used. A mix of several solvents is often used to combine several ideal qualities such as high fluidity and high dielectric constant. A high dielectric constant is needed to easily dissolve lithium salts, while a low viscosity ensure high mobility for lithium ions [12].

Solid electrolyte interface formation

The electrolyte is not stable at the potentials where lithium ions intercalate into the electrode. This leads to electrolyte decomposition at the electrode, forming a solid electrolyte interface (SEI). The onset potential of electrolyte decomposition has been disputed, but V=0.8 is the widely accepted potential for SEI formation [45]. However, it still varies with different electrolytes and electrolyte additives. The SEI prevents uncontrolled corrosion of the electrodes, consumption of the electrolyte and ensures kinetic stability of the electrolyte [12]. The formation of an SEI layer has two major down sides. First, Li-ions are consumed in the SEI formation process. As the amount of Li-ions in a cell is limited, the consumption of Li-ions may decrease the overall capacity of the cell. Second, if the SEI becomes too thick, it may limit the Li-ion transport through the layer. Optimally the SEI layer can minimize irreversible capacity (thus

increasing the energy density of the cell), increase cycling stability, rate capability and safety of the cell [40]. However, the SEI also increases the resistance in the cell, but this can be minimized by choosing the right solvents and salts for the electrolyte [46]. Carbon coating has been shown to lead to the formation of a uniform, thin and stable SEI layer on the electrodes [47], but can also cause excessive SEI formation.

1.2.3 Cathode

Cathodes, the positive electrode in a secondary battery, need to have a high potential versus the Li_0/Li^+ potential. As the anode materials used in LIB have a potential close to V=0 versus Li_0/Li^+, the operating voltage of the battery is determined by the cathode material utilized. This heavily influences the energy storage capability of the battery, and cathode potentials of close to 4 V is one of the main advantages of lithium ion batteries [40].

As with the anode material, a cathode should be able to insert and extract large amounts of lithium ions, be reversible and chemically stable at all lithium ion concentrations. Lightweight and environmentally friendly materials are also favoured [12].

1.2.4 Separator

The separator in a battery separates the electrodes physically, while ensuring free ion flow and preventing electronic flow. Porous and insulating semi-crystalline polymers such as polyethylene and polypropylene are commonly utilized. They have a melting point of respectively 130 °C and 165 °C. Therefore inorganic composite separators are chosen for applications that require high thermal stability, such as electric vehicle applications [12].

1.2.5 Current collector

The common current collectors used in LIBs are copper and aluminum foils for respectively the anode and cathode. Both contain an oxide layer on the surface protecting them from the corrosive effects of the electrolyte. However, salt electrolyte additives such as imide salt will lead to corrosion on the aluminum electrode, and HF impurities in the electrolyte will make the copper foil unstable. This must be taken into account when assembling a lithium ion battery. The weight of the metal foils, especially the copper foil, should be minimized as it decreases the gravimetric energy density of the battery [31].

1.3 SiO_2 anodes in lithium ion batteries

Various metals such as tin [47], germanium [48, 49], antimony [50] and metal oxides such as tin oxides [51, 52], manganese oxides [53], cobalt oxides [54] and iron oxides [55] have been researched as LIB anodes for their high theoretical capacity. The main disadvantage of these anode materials is their high volume variation during cycling. This volume variation during the lithium insertion/extraction process leads to pulverization of the anode and weakens the connection between the anode and the current collector [56]. In contrast silica anodes have been reported to exhibit both high capacity and good cycling stability [26].

Gao et. al. reported an electrochemical reaction between lithium and silicon dioxide nanoparticles in 2001 [17]. The reaction occurred in the 0-1 voltage range, and sparked an

interest in the potential of silicon dioxide for use in LIB anodes. Depending on the lithiation mechanism, the theoretical reversible capacity of silicon dioxide can be as high as 1961 mAh/g [14]. Because silica, or silicon dioxide, is the most abundant compound found in the earth's crust [16], it is easily accessible and cheap.

Generally, silica is nonreactive, dielectric and not an intercalating compound. However, as Gao et. al. discovered, the electroactivity increases with a decreasing size [17]. And the material becomes more applicable to battery production. Yang et. al. found the reversible capacity of SiO_x compounds (x $<$1.1) to decrease with decreasing oxygen content [57].

A comparison of different silica anodes can be seen in Table 1.2. Most show higher capacities than the theoretical limit of graphite anodes. However, it is apparent that the capacity decreases rapidly with increasing current, so from the research done so far there is limited possibilities for high power application.

Table 1.2: Specific capacities achieved with silica anodes in LIBs

Anode	Capacity [mAh/g]	Load	Voltage [V]
Silica thin film [13]	465	28 µA cm^{-2}	0.01-3
Nanosilica and hard carbon composite [14]	630	0.1 mA/cm	0.0-3
Pyrolysed red algae and diatoms [19]	530	18 mA/g	0.01-3.2
Hollow silica spheres [58]	980 - 350	0.6 mA cm^{-2}	0.0-2.5
Hollow silica cubes [59]	919	100mA/g	0-3.0
Carbon coated silica particles [25]	536	50 mA/g	1.0-3.0
Milled silica [18]	800	100 mA/g	0.0-2.0
Nanosilica carbon composite [24]	620	100mA/g	0.0-3.0
Carbon coated boron doped porous silica [15]	1400	1 A/g	0.01-2.0
Carbon coated boron doped porous silica [15]	1000	2 A/g	0.01-2.0

Due to the low standard redox potential of the Li_0/Li^+ redox couple, the silica anode acts as a cathode in a half cell configuration. This is because the lithium metal counter electrode has a lower potential, and thus becomes the negative electrode. However, since silica would be the negative electrode in a full cell configuration, it is referred to as the anode.

Half cells are utilized in research as the results are easier to compare when the same counter electrode is used, and because lithium metal provides a near limitless supply of lithium ions.

Carbon coating

In addition to mixing carbon to the active material, carbon coating of active materials can be used to improve the properties of the electrode. Carbon coating improves the electrical connection between the current collector and the active material, whereas a carbon additive only would create point contacts with the active material. This is a great advantage for electrodes with low electronic conductivity, whereas an electrode with a low ionic conductivity would benefit from a coating with a high ionic conductivity [60]. Carbon coatings may also be utilized to increase the stability of the electrode/electrolyte interface, which improves the cycling stability of the battery [15, 47].

The carbon source of the coating can be a carbohydrate [25], aquatic biomass [19] or an organic compound [61]. Pyrolysis of photoresist showed that the resistivity of the coating decreased dramatically when the pyrolysis temperature increased from 700 °C to 1000 °C [61].

Lithiation of SiO_2

Reversible lithiation of silica formimg $Li_2Si_2O_5$, described by Equation (1.7), has been affirmed using selected area electron diffraction (SAED) and X-ray photo-electron spectroscopy (XPS) [13]. However, the theoretical discharge capacity of Equation (1.7) is 357.3 mAh/g. Sun et. al. found the reversible discharge capacity to be 465 mAh/g, and suggested another contribution to the capacity might come from Si-Li alloy/dealloying process described in Equation (1.10) [13].

Experiments done on nano-silica by Guo et. al. has shown with NMR and XRD that Li_2O and Li_4SiO_4 is formed irreversibly during the initial cycle [14]. The reactions are described by Equation (1.8) and Equation (1.9), and account for the low coulombic efficiency during the initial discharge. The theoretical capacity of Equation (1.8) and Equation (1.10) together is 1965 mAh/g, and the theoretical capacity of Equation (1.8) alone is 983 mAh/g. Thus there is likely contribution form Equation (1.10) as reversible capacities of 1675 mAh/g has been achieved [14].

$$5\,SiO_2 + 4\,Li^+ + 4\,e^- \longleftrightarrow 2\,Li_2Si_2O_5 + Si \tag{1.7}$$

$$SiO_2 + 4\,Li^+ + 4\,e^- \longrightarrow 2\,Li_2O + Si \tag{1.8}$$

$$2\,SiO_2 + 4\,Li^+ + 4\,e^- \longrightarrow Li_4SiO_4 + Si \tag{1.9}$$

$$Si + xLi^+ + xe^- \longleftrightarrow Li_xSi \tag{1.10}$$

Alloying of Si and Li (Equation (1.10)) is assumed to be a co-reaction increasing the specific capacity of silica anode LIBs. This reaction only occurs at above 700 K with Li and Si as bulk materials . When alloying with nano silicon however, the reaction is viable at 300 K. This gives reason to believe the reversible alloy formation occurs in silica anodes [17].

1.4 SiO_2 from coscinodiscus diatoms

Diatoms are unicellular or colonial eukaryotic algae with unique cell walls consisting of amorphous silica [16]. These cell walls, called frustules, contain a regular patterning down to the nanometer range, and contribute to the effective photosynthesis of the diatoms [62]. More than 10 000 species of diatoms are known, and there is expected to exist many more. They are abundant in the marine and fresh water ecology, and they account for approximately 25 % of the worlds net primary production [20]. The worlds net primary production is the worlds synthesis of energy from atmospheric or aqueous CO_2.

The nanostructuring of the frustule has many possible applications. The high ordering of the frustule makes the diatom a living photonic cell [63]. This has been exploited in making gas sensors [64], solar cells [65], and in electroluminescent displays [66]. The silica frustule can be used as a high surface area LIB anode [19].

Coscinodiscus diatoms are a family of centric diatoms. This means that their frustules have a radial symmetry. Figure 1.3 shows a scanning electron microscope (SEM) image of the symmetric coscinodiscus walesii frustule.

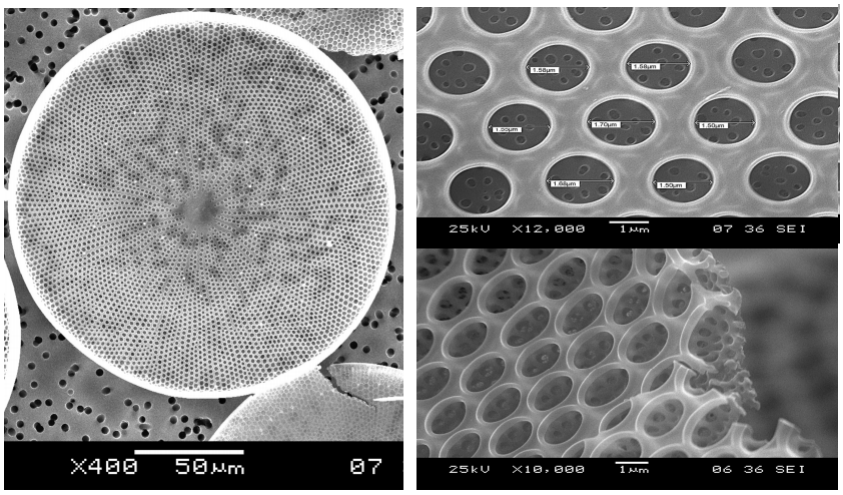

Figure 1.3: SEM images of coscinodiscus diatoms with scalebars of respectively 50 µm and 1 µm. Adapted from De Stefano et. al. [67].

1.5 Characterization methods

Raman spectroscopy

Raman spectroscopy is a vibrational technique providing data on the chemical bonds in a material on the atomic scale. The technique uses monochromatic light which scatters when it reaches the material. Most of this light will scatter at the same frequency as the incident light, Rayleigh scattering, and some of it will scatter at different frequencies due to the vibrational state of the molecule, Raman scattering. The inelastic Raman scattering is measured, and the difference in energy between the incoming photon and the scattered photon gives the vibrational energy of the molecule [68].

Graphite has a characteristic raman peak at 1580 cm^{-1} called the G band. This peak is a result of the C-C streching mode in graphite crystals. Disordered graphite display a raman peak at 1350-1360 cm^{-1} called the D band. This peak is from C-C stretching in sp^3 hybridized carbon, which is the bonding found in diamond structured carbon. In graphite a D band peak formation is linked to disorder along the c-axis of the crystal, defects, polycrystallinity and discontinuity [69]. The ratio of the intensity of the D band, I_D, and the intensity of the G band, I_G, is inversely proportional to the crystallite size of a graphite crystal. However, the intensities of carbonaceous materials are dependent on both the exitation wavelength and laser energy utilized. Thus, the intensity ratio only gives an indication of the crystallite size [69].

In amorphous carbon, the D band intensity is linked to ordering of the structure, as it suggests increased sp^3 bonding [70].

X-ray diffraction

X-ray diffraction (XRD) is the elastic scattering of X-rays in crystalline materials. Diffraction occurs when the wavelength of an X-ray is the same order of magnitude as the distance between planes in a crystal. This creates interference, where most of the scattered waves are cancelled out by negative interference. However, at some angles there is positive interference which is

described by Braggs law:

$$2d \sin \Theta = n\lambda$$

where d is the distance between crystallographic planes, Θ is the angle at which the X-ray beam is diffracted, n is an integer and λ is the wavelength of the beam.

This can be used to determine the constituents of a crystal, find the lattice parameters, and determine if a product has become crystalline or not [71].

Thermogravimetric analysis

Thermogravimetric analysis (TGA) is a method that examines the pyrolysis, combustion and high temperature behavior of materials. This is performed by heating the sample at a linear rate in a chosen atmosphere while continually recording weight changes. The athmosphere can be changed determining the type of measurement done [72].

Nitrogen adsorption

Nitrogen gas adsorption is a characterisation technique where physisorption of nitrogen molecules on the surface of an adsorbate/sample material is used to determine the surface area of the adsorbate/sample material. In 1938 Brunauer–Emmett–Teller (BET) theory was developed to take into account the formation of multilayers on the adsorbates surface to better describe the process [73]. With porous materials the nitrogen molecules also adsorb into the pores on the adsorbate, and continue to fill these pores. Barrett-Joyner-Halenda (BJH) theory takes into account the adsorption rate based on the size of the pores, and can give a pore size distribution of the adsorbate [74].

Galvanostatic cycling

Galvanostatic cycling is used in battery research to test running conditions, stability and performance over time for a battery. This is done by applying a constant specific current (current density) over a defined potential window, while measuring the potential over the battery. This is done over a defined potential window. Based on current, the time it takes for the battery to reach the lower cut-off potential, and the mass of the active material, the capacity can be estimated. The rate capability can be analyzed by changing the specific current. Stability and lifetime expectancy can be analyzed by repeated cycling over long periods of time. The efficiency of the battery can be calculated by comparing the differences in capacity between charge and discharge.

2. Materials and methods

2.1 Overview

This chapter will describe in detail the experimental procedures, materials and characterization techniques used in this project. From the extraction of silica from diatoms to the electrochemical characterization of coin cells with the silica (SiO_2) anodes. The section is divided into two parts. It starts with a section describing all the experimental procedures and the second section is a description of all the characterization techniques.

The frustules of the diatoms consists of amorphous silica, which was obtained by washing and calcination of the diatoms. This process removes the organic material, so only the pure amorphous silica frustules of the diatoms remain. The silica was then milled into a fine powder and carbon coated with sucrose as the carbon source. Sucrose was converted into a carbon coating by pyrolysis in an argon atmosphere between 650 °C -1050 °C. Five more carbon coated silica samples were made with 20-100 wt% sucrose content and pyrolysed at 1050 °C in an argon atmosphere.

The pyrolysed carbon coated silica samples were then analyzed by TGA to find the individual carbon content, and by nitrogen adsoption to find the surface area. The carbon and silica samples and an additional pure milled silica sample were then mixed with alginate and carbon black and cast as electrodes onto a copper current collector. Electrodes were punched out and assembled into coin cells with lithium metal as the counter electrode for galvanostatic cycling to obtain the electrochemical properties.

2.2 Electrode preparation and coin cell assembly

2.2.1 Washing and calcination of diatoms

The received diatoms from Planktonic AS contained oils, seawater and other impurities. Thus, they have to be washed before the organic matter can be removed by calcination. This is because the inorganic impurities will not burn off during the calcination.

First, the as recieved diatoms were left in a beaker for one hour to separate the diatoms from the oils. Then they were separated using a 32 µm mesh sieve and rinsed with DI water to remove most of the oil. After this, the diatoms were dried in a heating cabinet at 90 °C for 24 hours, followed by 150 °C for 24 hours.

The dried diatoms were mixed with DI water with a 1:100 mass ratio and heated to 130 °C on a hotplate while stirring at 500 rpm with a magnetic stirrer for two hours. Following, the diatoms and the DI water were separated using a 32 µm mesh sieve and rinsed in DI water. Again the diatoms were mixed with DI water with a 1:100 mass ratio, and sonicated for 30

minutes at 25 °C in an ultrasonic bath.

Finally, the diatoms were separated from the DI water using a 32 µm mesh sieve, rinsed under running DI water for 5 minutes, and dried in a heating cabinet at 90 °C for 24 hours followed by 150 °C for 24 hours.

Calcination of the dried diatoms was conducted at 650 °C for four hours under a synthetic air atmosphere (80 Lh^{-1}).

2.2.2 Planetary milling of calcined diatoms

Planetary milling was performed with a PM100 planetary mill from Retsch. The milling of the calcined diatom powder was performed in two sessions where the rotary direction was changed between intervals. The powder was milled in a stainless steel 50 mL jar with 4 stainless steel balls (4g, 10 mm) at a 1:12 ball to powder mass ratio. In the first milling session the powder was milled at 600 rpm for 90 minutes with 5 minute intervals and 10 second breaks between intervals. For the second session the powder was milled for 40 minutes at 600 rpm with 10 minute intervals and 5 minutes break between each interval. The reason for doing the milling in two sessions was because the process was still being optimized, and changing the rotary direction between intervals improves the homogeneity.

2.2.3 Carbon coating

Carbon coating of the milled diatom powder was produced with sucrose in the following manner, with different silica and sucrose content according to Table 2.1. The desired amount of sucrose was mixed with 2-4 g of DI water and lightly stirred until all the sucrose was dissolved. Then the milled diatom powder was added to the solution and sonicated for 30 minutes at 25 °C in an ultrasonic bath. To evaporate the DI water the mixture was heated to 60 °C on a hotplate while stirring with a magnetic stirrer at 250 rpm. When most of the DI water had evaporated, after one to two hours, the mixture was added to a mortar and grinded for approximately five minutes until becoming a white/gray powder. The sucrose and silica powder was added to an alumina crucible and pyrolysed in a furnace at 650-1050 °C, as listed in Table 2.2.

Table 2.1: Amount of silica and sucrose added to each electrode

Sample name	Silica content [wt%]	Sucrose content [wt%]
PMCC1050-20	80	20
PMCC1050-40	60	40
PMCC1050-60	40	60
PMCC1050-80	20	80
PMCC1050-100	0	100

2.2.4 Preparation of alginate binder

The alginate binder was prepared with sodium alginate from brown algae (Na-Alg, 100 g, Sigma Aldrich) and DI water. They were mixed with a 1:60 mass ratio and heated to 60 °C on a hotplate while stirring at 500 rpm for 4 hours.

Table 2.2: Pyrolysis temperatures

Sample name	Pyrolysis temperature [°C]
PMCC650	650
PMCC700	700
PMCC750	750
PMCC800	800
PMCC850	850
PMCC950	950
PMCC1050	1050

2.2.5 Electrode casting

The electrode slurry was prepared by mixing 35 wt% carbon black, 15 wt% alginate binder and 50 wt% active material. The active material used was mixtures of carbon coated silica and pure carbon listed in Table 2.2, and a reference of milled diatoms that had not been heat treated after the calcination.

Mixing of the slurry was conducted by ball milling (NM 400 mill, Retsch) at 25 Hz for 45 minutes. Then it was cast onto a copper current collector (18 µm BF PLSTR, circuit foil luxembourg) using a tape caster (model K101, The K control coater) and a coating head calibrated to give a 40 µm thick wet film. After casting, the electrodes were dried in a heating cabinet at 70 °C. Then they were dried in a vacuum drying chamber (VD23, Binder) at 120 °C overnight to remove excess moisture.

Immediately after drying, the 16 mm diameter electrodes were punched out from the cast, weighed and stored in a glove box.

2.2.6 Coin cell assembly

The coin cells were assembled with 20 mm CR2016 stainless steel 304 coin cell cases. The electrolyte constituted of 1M $LiPF_6$ dissolved in a 1:1 mixture of ethylene carbonate and diethyl carbonate.

Assembly of the coin cells was conducted in an Ar glove box with H_2O and O_2 values of less than 0.1 ppm during the whole process. The assembly was conducted as demonstrated in Figure 2.1. First the carbon coated silica anode was placed on the bottom of the coin cell with the current collector facing down. Then 20 µL of electrolyte was added, the separator (Celgard 2400, 20 um thick, Celgard) was put on top and an additional 20 µL of electrolyte was added. Then a 14 mm diameter counter electrode of lithium-foil (99.9 %, 0.75 mm thick, Alfa Aesar) was punched out, brushed to remove oxide and added to the coin cell. The 16 mm x 0.3 mm spacer (SUS316L) and cell cap was added and finally, the cell was sealed with a crimping tool (Automatic crimping machine, Hohsen Corp) .

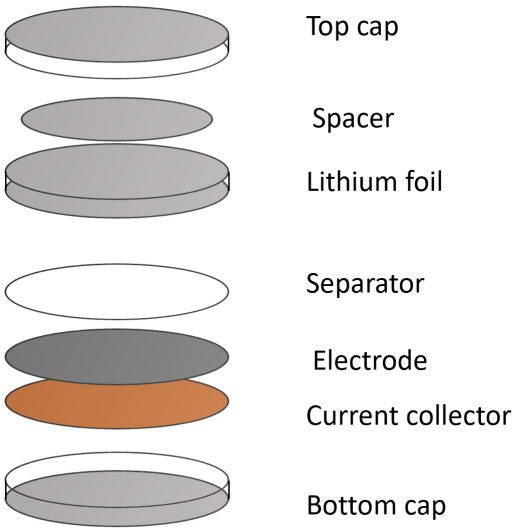

Figure 2.1: Illustrated assembly of coin-cells.

2.3 Characterization methods

2.3.1 RAMAN spectroscopy

RAMAN spectroscopy was conducted with a WITec Alpha300 R with an intensity of 1.5 mWh. This was done to ascertain if the carbon coating was graphitized, and also to investigate any effect on the carbon coating of increasing calcination temperature. For each sample, two measurements were conducted in different spots to make sure the individual measurement was not an anomaly. The individual measurements were conducted as an average of 20 measurements of 0.5 seconds.

2.3.2 X-ray diffraction

X-ray diffraction (XRD) was done with a D8Focus with Cu Kα radiation and a Lynxeye detector. This was done to see if the carbon coated silica pyrolysed between 650 °C and 1050 °C became crystalline. The samples were measured with 2976 measurements of 0.5 seconds between 2Θ values of 5 and 90.

2.3.3 Thermal gravimetric analysis

Thermal gravimetric analysis (TGA) was done with a Netzsch STA 449 C. This was conducted to ascertain the carbon content of the active material in the different electrodes. The sample of carbon coated silica was analyzed using a heating rate of 10 °C per minute until reaching 1000 °C and kept there for 120 min.

2.3.4 Nitrogen adsorption

Brunauer–Emmett–Teller (BET) and Barrett-Joyner-Halenda (BJH) analysis was conducted with a 3Flex 3500 after degassing for 10 hour at 240 °C in a nitrogen atmosphere. This was performed to find the surface area and pore size of the carbon coated silica pyrolysed at different temperatures. Because these properties heavily affect the cyclic properties of the electrode, it was important to know if the pyrolysis temperature would affect the surface area and pore size of the material.

2.3.5 Galvanostatic cycling

Galvanostatic cycling was done on a BioLogic BCS-805 galvanostat and a Lanhe CT2001A battery testing system to find the electrochemical cycling behaviour of the cells. The cycling was conducted between 0.002 V and 2.0 V. The formation cycle was conducted with a current density 10 mA/g and the subsequent cycles were run at 50 mA/g.

3. Results

3.1 Effect of increased pyrolysis temperature

Silica characterization

XRD results of carbon coated silica samples pyrolysed at different temperatures are displayed in Figure 3.1. All samples display a broad peak between 20-25 degrees. PMCC1050 displays a tendency to a peak at 24 degrees.

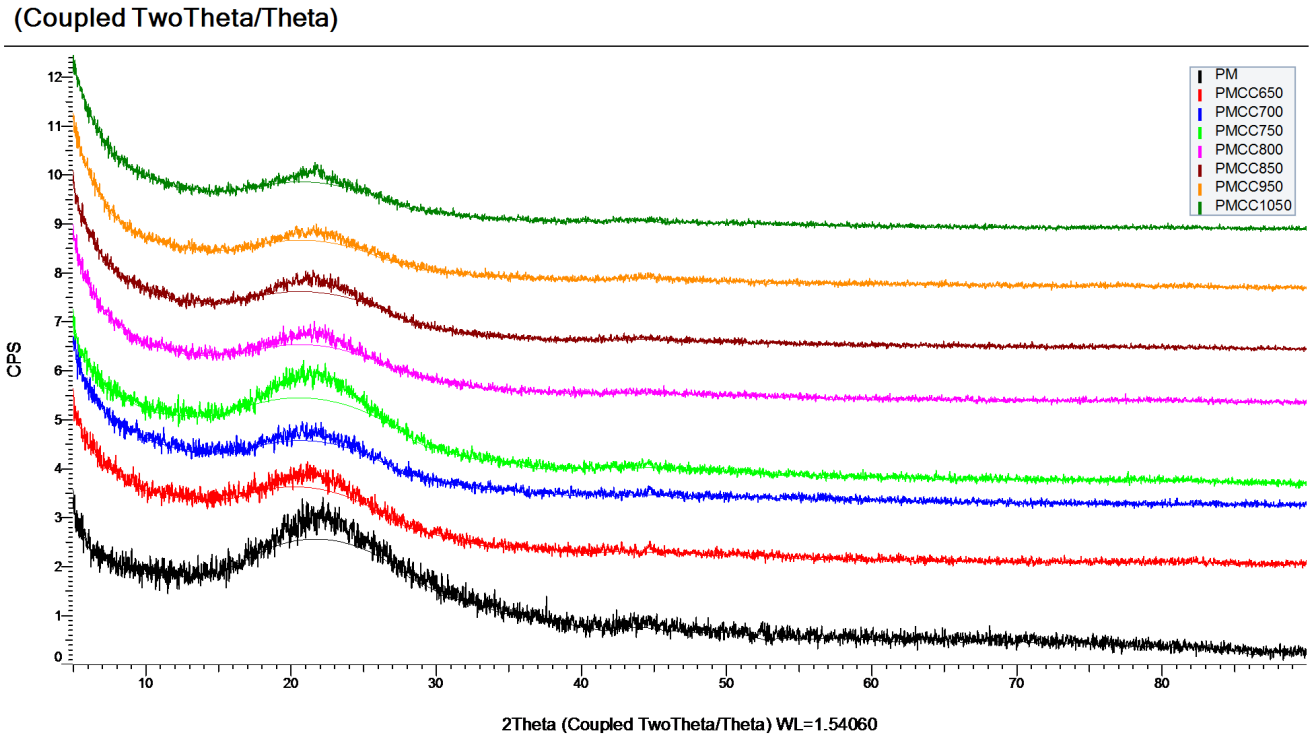

Figure 3.1: XRD results for carbon coated silica pyrolysed at different temperatures.

Surface area and porosity

Table 3.1 displays the surface area and average pore diameter of carbon coated silica samples pyrolysed at 650 °C, 850 °C and 1050 °C. As a reference milled and unmilled silica from diatoms is supplied from Norberg et. al. [28]. The measured pore size and micropore contribution decreases slightly. However, the surface area of PMCC1050 is drastically reduced.

Table 3.1: Surface area, micropore area and average pore diameter.

Sample name	Surface area [m^2/g]	Micropore area [%]	Average pore diameter [Å]
Silica	8.19	58.1	1509
Milled silica	17.7	25.2	1533
PMCC650	257.7	85.6	35.67
PMCC850	220.82	85.5	32.00
PMCC1050	62.41	80.5	29.92

Carbon characterization

The raman spectroscopy performed on carbon coated silica pyrolysed at different temperatures can be seen in Figure 3.2. All of the raman spectra display broad D bands and G bands. As the pyrolysis temperature increases the D/G band intensity ratio increases which can also be seen in Figure 3.4. As one of the measurements deviated a lot from the others, two graphs have been plotted. Figure 3.4a and Figure 3.4b without and with the outlier respectively. Figure 3.3 displays the raman spectra of graphite with defined peaks at 1581.8 cm^{-1} and 2716.9 cm^{-1}. Smaller peaks are seen at 2446.3 cm^{-1} and 3242.4 cm^{-1}.

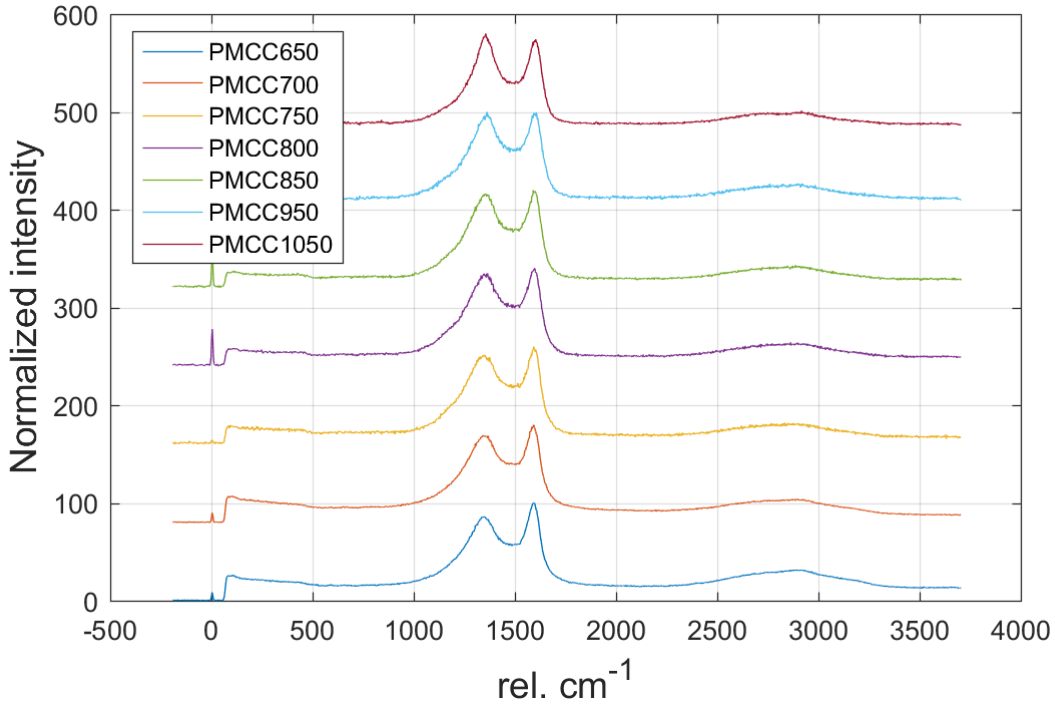

Figure 3.2: Raman spectrum of carbon coated silica pyrolysed at different temperatures.

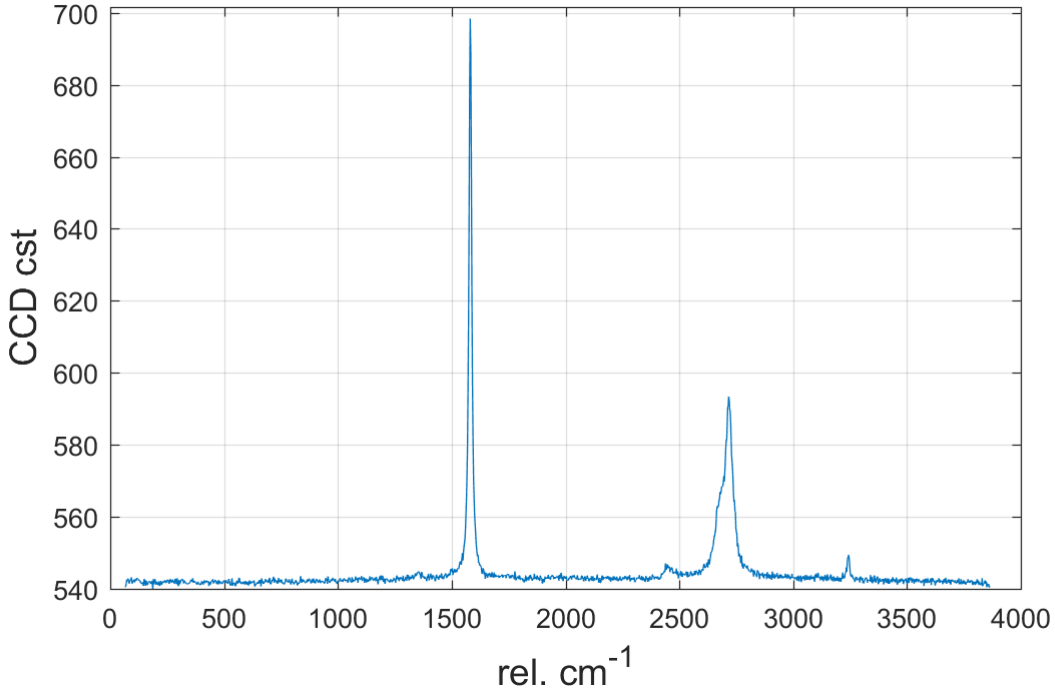

Figure 3.3: Raman spectrum of graphite.

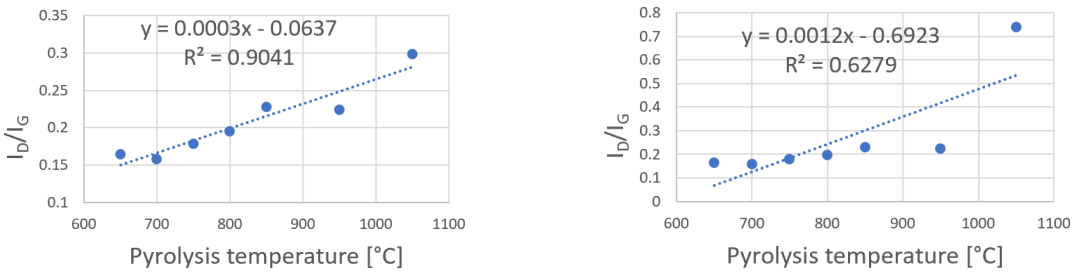

(a) (b)

Figure 3.4: Ratio of the D and G band intensities versus the pyrolysis temperature. Figure 3.4a displays the intensity ratio without the outlier while Figure 3.4b displays the intensity ratio with the outlier.

3.2 Characterization of active material

Silica characterization

Figure 3.5 display XRD results of carbon coated silica samples pyrolysed at 1050 °C with different wt% of carbon precursor. As the carbon content decreases a peak formation at 23 degrees is observed.

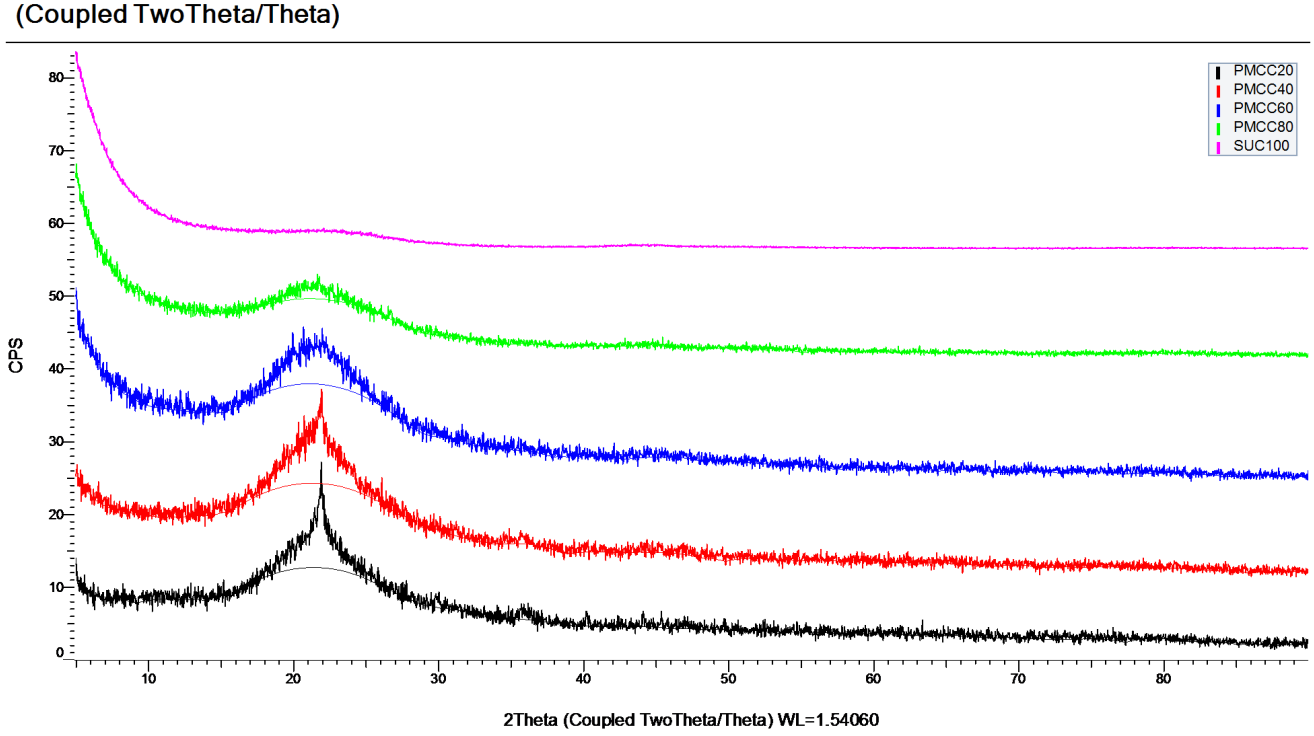

Figure 3.5: XRD for carbon coated silica with different carbon content.

Detection of carbon content

TGA measurements revealed the carbon content of the carbon coated silica samples with known sucrose content pyrolysed at 1050 °C. The measured data is listed in Table 3.2, and fitted to a curve in Figure 3.6 .

Table 3.2: Measured carbon content in carbon coated silica with altered sucrose content.

Sample name	Carbon content [wt%]
PMCC20	4.8
PMCC40	13
PMCC60	29
PMCC80	49
PMCC100	100

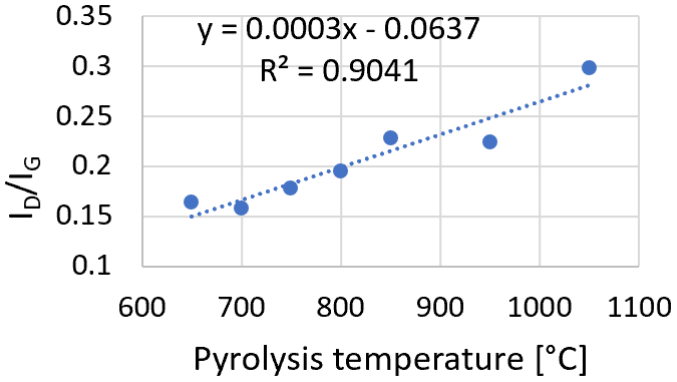

Figure 3.6: Carbon content versus carbon precursor content with a fitted curve. The sucrose is mixed with silica before pyrolysing to obtain carbon.

Carbon characterization

Raman spectroscopy of the samples pyrolysed with different wt% sucrose can be seen in Figure 3.7. Not showing detectable differences between the samples with altered carbon content.

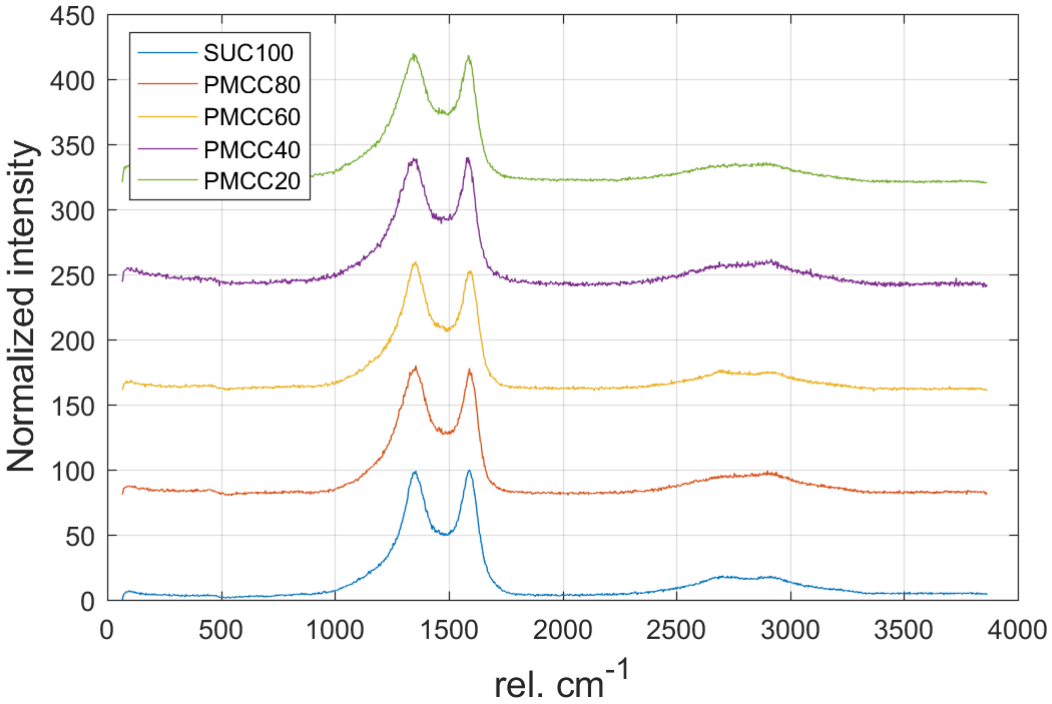

Figure 3.7: Raman spectroscopy of carbon coated silica with different carbon content.

3.3 Electrochemical properties

Figure 3.8 displays that the coin cell battery with the best capacity was the silica reference cell without carbon coating. For all the batteries containing silica the capacity increases with

increasing cycling. The carbon coated silica samples, PMCC20, PMCC40, PMCC60 and PMCC80, display a capacity peak in the first cycle. Potential profiles of the first discharge/charge cycle of the silica reference, PMCC20, PMCC80 and SUC100 are displayed in Figure 3.10. All have a plateau at V=0.9, and the silica cells have a plateau close to V=0.02 . The V=0.02 plateau of Figure 3.10a is significantly larger than the one in Figure 3.10b, and decreases further for Figure 3.10c.

Figure 3.9 displays the loading of the cells. The loading of the silica reference cell is significantly lower than the loading of the carbon coated cells.

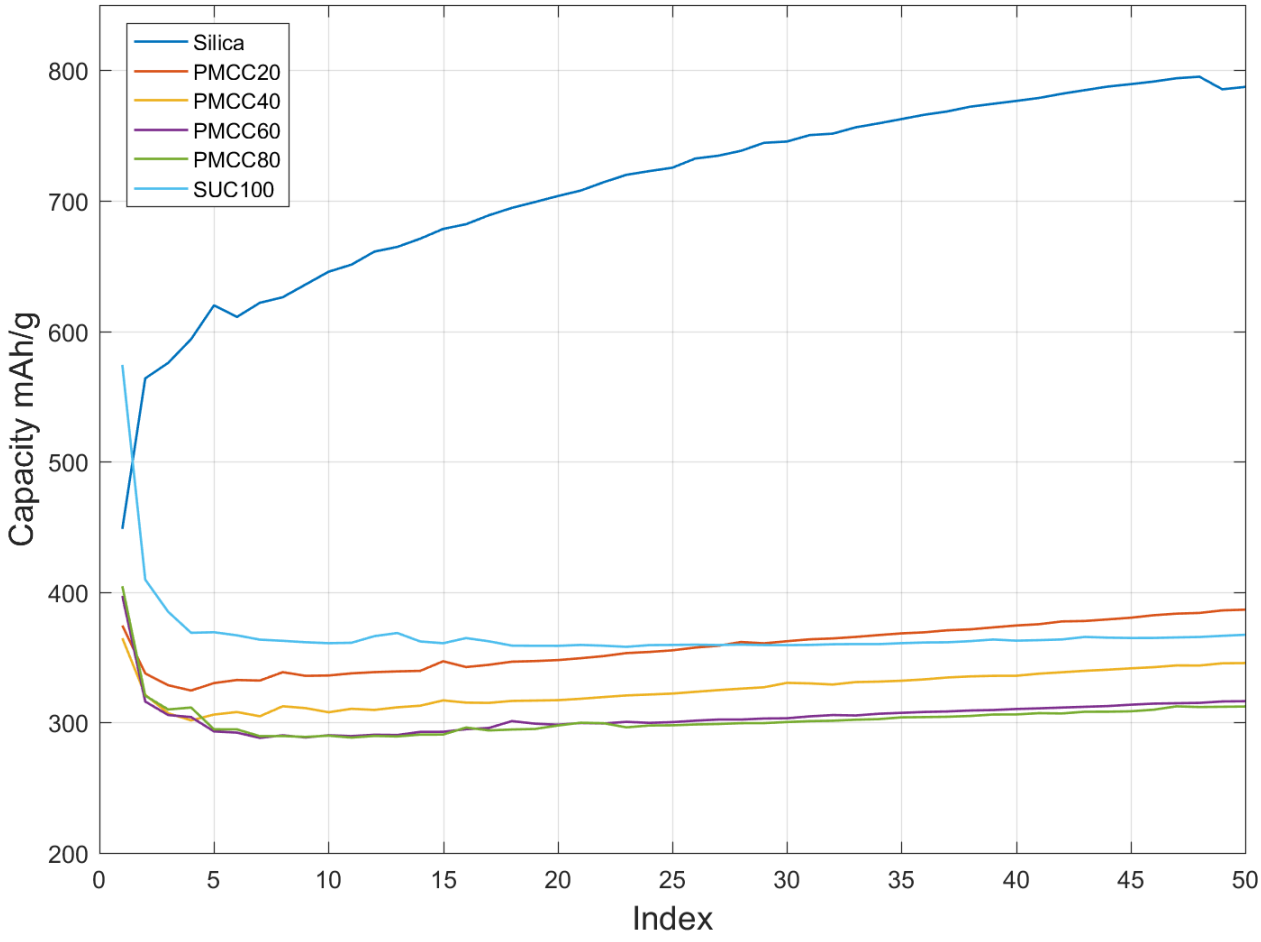

Figure 3.8: Specific charge capacity versus cycle number.

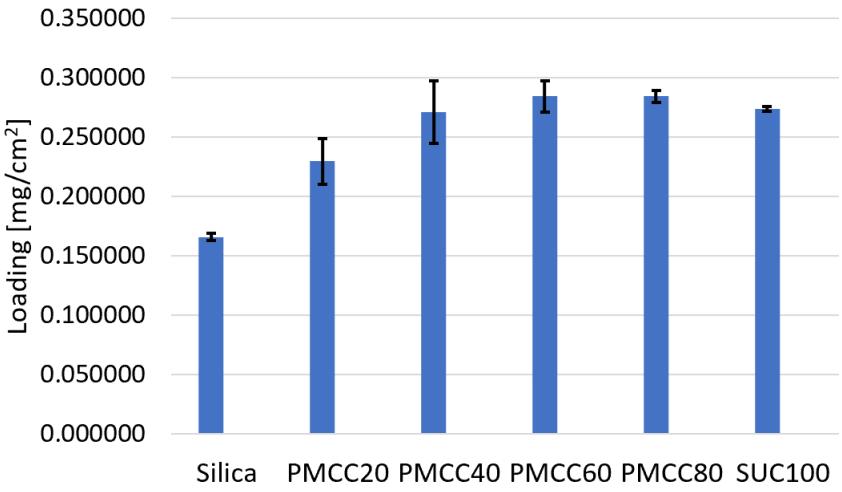

Figure 3.9: Loading of cells with different carbon content, with error bars indicating standard deviation.

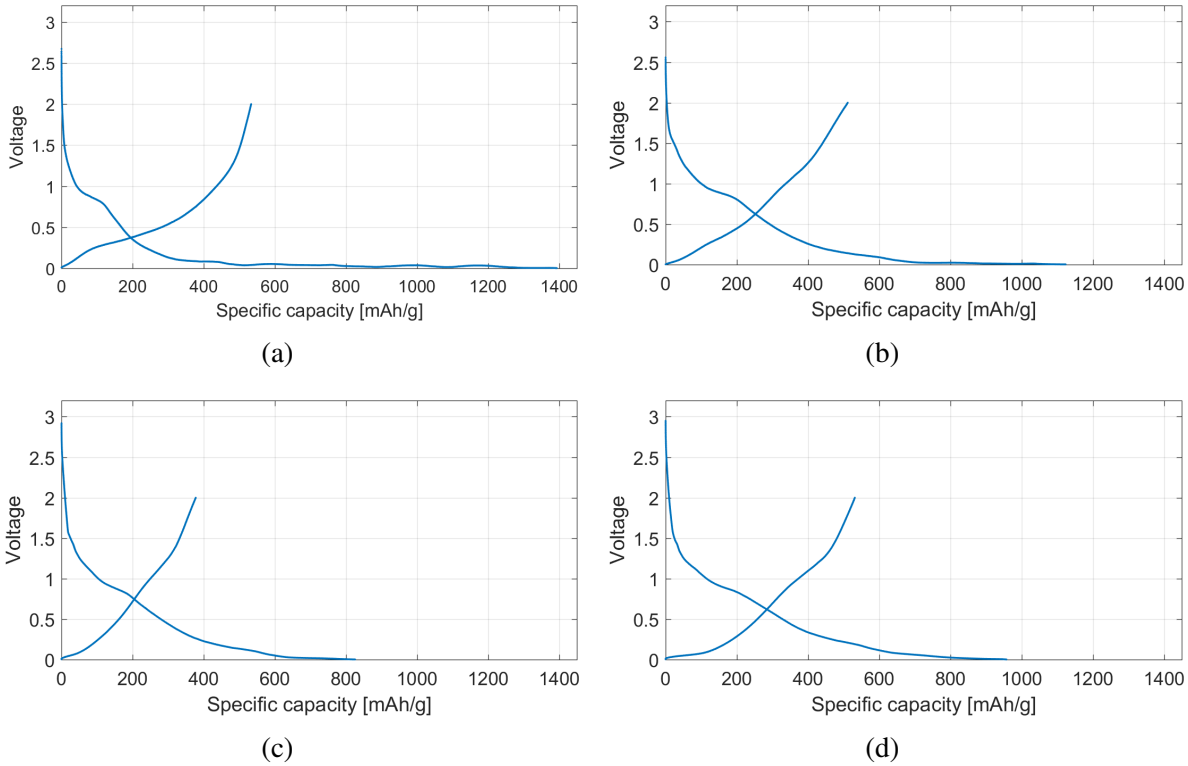

Figure 3.10: Potential profiles of the first discharge and charge cycle. (a) displays the milled silica reference battery, (b) displays sample PMCC20, (c) displays sample PMCC80 and (d) displays sample SUC100.

4. Discussion

4.1 Effect of increased pyrolysis temperature

Silica characterization

In Figure 3.1 the broad peak at 20-25 2Θ is attributed to the presence of amorphous silica. This conveys that the higher pyrolysis temperatures have not caused the silica to become crystalline. This is favorable for the production of batteries as an amorphous structure is necessary for the lithium ions to penetrate into the structure [18]. Low crystallinity and high porosity of silica has shown to be beneficial for lithium ion batteries [15]. However, there are signs of a peak formation at 24 degrees in PMCC1050 pyrolysed at 1050 °C, which may indicate some ordering of the silica. PMCC650 might have a peak attributed to carbon ordering at 45 2Θ. This peak is not present in the pyrolysed sucrose sample SUC100 in Figure 3.5, and suggests the minor peak in PMCC650 is due to the signal to noise ratio in the measurements of amorphous silica.

Carbon properties

The D and G band in Figure 3.2 indicate that the pyrolysed sucrose carbon coating has characteristics of glassy amorphous carbon [69].

The I_D/I_G ratio in Figure 3.4 increases with increasing pyrolysis temperature. This indicates an increase in electrical conductivity of the carbon with increasing pyrolysis temperature, in accordance with the findings of Kostecki et. al. [61]. It also indicates an ordering of the carbon substanciated by the decrease in surface area with increasing pyrolysis temperature (Table 3.1). The outlier in Figure 3.4b is not taken into account, as the other measurements show a clear trend.

Surface area and porosity

The surface area decreases drastically as the pyrolysis temperature changes from 850 °C to 1050 °C (Table 3.1), indicating a drastic change in the properties of the carbon coating. The micropore percentage of the area and the average pore size decrease slightly, but not to the same degree as the surface area. This implies a thinning and compacting of the carbon coating. Decreased surface area in high crystalline graphite correlates to a decrease in the irreversible capacity [40]. However, as the carbon coating consists of glassy carbon it might behave differently. A decrease in the surface area is beneficial as it provides the SEI layer a smaller surface on which to form.

The micropores contribute significantly to the total surface area although the contribution has decreased from 85 % to 80 %. This can have a detrimental effect to the capacity of the battery as lithium ions cannot penetrate pores smaller than 2 nm (micropores).

This indicates that the carbon properties were enhanced by increasing pyrolysis temperature to 1050 °C, as both the surface area decreased and the electrical conductivity increased.

4.2 Characterization of active material

The absence of potassium, chlorine, sodium or any other crystalline peaks in the XRD measurements in Figure 3.1 and Figure 3.5 confirm the successful washing of the diatoms prior to calcination.

Figure 3.5 displays a peak developing as the carbon content decreases. This suggests minor ordering of the silica at 1050 °C. The peak development with decreasing carbon content might occur because the silica signal is stronger with a thinner carbon layer.

Carbon content

As expected the carbon content after pyrolysis is lower than the initial sucrose content. Yao et. al. found the optimal carbon coating content of silica nanoparticles to be 50 % carbon [25]. However, a thinner carbon layer, thus a lower carbon content, might be beneficial if it promotes a thinner SEI. This would lead to a more electrically and ionically conducting electrode.

Figure 3.6 displays a curve fitted to the carbon content data. The exponential curve fits with the data, but is likely to change with more data for sucrose contents below 20 %. This is because the fitted curve does not approach 0% as the sucrose content goes to 0 %.

Carbon properties

The raman spectrum of graphite, seen in Figure 3.3 has a clear G band peak and no D band peak. Comparing Figure 3.7 and Figure 3.2 with Figure 3.3, the absence of sharp peaks at the G and D band in Figure 3.2 and Figure 3.7 indicate that the structures are not graphite.

Figure 3.7 display the raman spectroscopy of samples with different carbon content. They contain the same intensities and peaks indicating that the carbon properties do not change with carbon content.

4.3 Electrochemical properties

The coin cells produced are half cells, which make the charge capacity an important characteristic. This is because in a full cell this is the discharge capacity of the battery.

In Figure 3.8 we see that the silica reference cell has a distinct capacity profile compared to the carbon coated silica cells and the pure carbon cell. The cells containing pyrolysed carbon have a significant capacity loss during the first cycles which can be attributed to SEI formation in the carbon. The silica reference cell on the other hand displays a drastic increase in the first cycles, and a gradual increase with increasing cycling number.

The pure silica reference cell has a high initial capacity of 448 mAh/g, increasing to 790 mAh/g at cycle 50. The carbon coated silica shows an initial capacity ranging from 364 mAh/g to 404 mAh/g, lower than the pure carbon cell which displays the highest initial capacity at 574. After the initial capacity loss the pure carbon cell displays a stable capacity at approximately 367 mAh/g, while the capacity of the carbon coated silica cells increase with cycling number. At cycle 50 the capacity of the carbon coated silica cells ranges between 312 mAh/g and 386

mAh/g at cycle 50. The PMCC20 cell displays a capacity of 386 mAh/g and is the only carbon coated cell with a capacity exceeding that of the pure carbon. The carbon coated cells display a significant increase in capacity as the carbon content decreases.

Capacity contribution from carbon

The high capacity of SUC100 suggests that the carbon in the carbon coating contributes significantly to the capacity of the anode. The raman spectroscopy results show that the active material consists of amorphous carbon, which has been shown to have capacities up to 1000 mAh/g [75]. However, because the capacity of the carbon coated silica cells increases as the carbon content decreases, the silica contributes more to the capacity than the carbon content in the cells.

Carbon coating

In Figure 3.8, the capacity of the silica reference cell is almost twice as high as the PMCC20 cell, which has the highest capacity of the carbon coated silica cells. This observation may be explained by two different mechanisms. First, the pure silica reference has almost half the loading than of the carbon coated silica samples (Figure 3.9). Second, the carbon coating may result in a thicker SEI layer hindering the conversion of silica to silicon in accordance with the reactions in equations (1.7) to (1.10). The surface area of milled silica is drastically lower than the surface area of the carbon coated silica (Table 3.1), which will contribute to excessive SEI formation in the carbon coated silica anodes.

Effect of SEI formation

The potential profiles of the cells in Figure 3.10 display the affects of carbon coating. All the cells have a plateau at V=0.9 corresponding to formation of the SEI layer. This plateau is significantly broader as the carbon content increases, indicating a thicker and/or larger SEI layer due to carbon coating. The increased electrolyte decomposition can be explained by the increased surface area on the carbon coated silica cells, as the carbon content contributes significantly to the surface area of the anode (Table 3.1).

The potential profiles (Figure 3.10) of the cells display an additional plateau at V=0.02. This equilibrium plateau contributes significantly to the capacity of the silica reference sample (Figure 3.10a) indicating that it corresponds to the lithiation reaction in the anode converting silica into silicon and storing lithium ions in the silicon by the reactions in equations (1.7) to (1.10) [13, 14]. Silicon has multiple lithiation potentials that are all below V=180 mV [76], which would concur with the proposed lithiation mechanisms [13, 14] and the obtained potential profiles. The length of this plateau decreases with increasing carbon content, corresponding to the decrease in capacity with increasing carbon content (Figure 3.8).

The increased thickness of the SEI layer for the carbon coated silica cells can both hinder the diffusion of lithium ions to the silica surface and cause an IR loss, resulting in both diffusion and electrical polarization. An increased polarization of the cell might shift the lithiation curve of reactions between silica and lithium, thus the silicon formation might not be occurring in the cycling window of the cell. The decrease in lithiation of the carbon coated silica cells is clearly displayed comparing the potential profile of the silica reference cell (Figure 3.10a) with PMCC20 Figure 3.10b. A further decrease in silica lithiation is observed with PMCC80 (Figure 3.10c), and is not present in the pure carbon cell (Figure 3.10d). This is corroborated by

Figure 3.8 where the capacity increase seen due to silicon formation is not as prominent in the PMCC60 and PMCC80 cells. Which suggest that the polarization due to SEI formation reduces the silicon conversion of the cells.

Another possible mechanism is the high micropore content. The carbon coated silica surface consist of 80.5 % micropores (Table 3.1) which can decrease the lithium mobility in the SEI layer significantly, thus increasing the diffusion polarization.

Effect of loading

As previously noted the different cells were subjected to the same specific current. However, the silica reference anode had a significant lower loading compared to the carbon coated silica anodes (Figure 3.9). Increased loading may increase the IR polarization, and thus shift the lithiation curve of the silica reduction mechanism. This effect could also be expected to be more prominent for silica electrodes, as the material is known for its poor electrical conductivity. Comparing Figure 3.9 and Figure 3.8, it is clear that the silica reference cell and the PMCC20 cell have both the highest capacities after 50 cycles and the lowest loading. However, the big difference between the capacities of the silica reference cell and the PMCC20 cell can not be explained by loading alone.

Effect of carbon content

The capacity of the carbon coated silica anodes with 60-80 % sucrose are surprisingly similar (Figure 3.8). As the carbon content varies from 29 % to 49 % (PMCC60 and PMCC80 from Table 3.2) there is little difference in the capacity after 50 cycles. This is not in accordance with Yao et. al. 2011 as they found the silica nanoparticles with 50 % carbon coating obtained the highest capacity. This is most likely because they did not take the carbon contribution of the capacity into account, thus the carbon contributed more than the silica to the increased capacity. This effect can also be explained by polarization due to loading, SEI formation and micropores. In Figure 3.9 PMCC40, PMCC60 and PMCC80 have similar loading values while the loading of PMCC20 is significantly lower. SUC100, on the other hand, has a comparably high loading, the highest carbon content and a high capacity. This suggests that the loading effects influence carbon coated silica anodes more than the pure carbon anode. Which may be because of the larger IR polarization due to the poor electronic conductivity of silica.

4.4 Final remarks on carbon coating of silica from diatoms

The increase in pyrolysis temperature of the carbon coated silica did appear to be beneficial to the properties of the carbon coating. However, the SEI formation in the carbon coated cells hamper the conversion of silicon in the cells.

The silica reference cell displayed promising results, but the poor conductivity of the material will result in IR losses at higher specific currents and/or loading. Carbon coating can benefit the conductivity, but to decrease the SEI formation a lower surface area is needed. This can be done by trying to increase the temperature further or by using a catalyst to graphitize the carbon at lower temperatures, while ensuring that the silica does not become crystalline.

Other improvements can be made by decreasing the carbon content in the carbon coating. The carbon coated silica cells displayed increasing capacities with decreasing carbon content. The carbon coated silica pyrolysed with a sucrose content of 20 % (PMCC20) did display a

higher capacity than the theoretical capacity of graphite after 40 cycles, which is promising. This suggests that an even lower carbon content might achieve higher capacities and more silicon conversion.

5. Conclusion

Optimization of carbon coating of silica from diatom frustules as an environmentally friendly anode material was attempted. Previous work on silica derived from diatoms has not displayed capacities comparable to what is reported on silica anodes in literature. Here, the anode performance was optimized by examining the effect of the pyrolysis temperature and carbon precursor amount.

Increasing the pyrolysis temperature from 650 °C to 1050 °C decreased the surface area and increased the I_D/I_G ratio of the carbon coated silica without crystallizing. This suggested less SEI formation and increased electrical conductivity of the active material as the temperature increased, without causing the silica to become crystalline.

Altering the carbon content of the carbon coated silica cells did not affect the carbon properties, but heavily affected the electrochemical properties of the prepared coin cells. There was a significant increase in capacity with decreasing carbon content. A capacity of 386 mAh/g after 50 cycles was achieved with a carbon content of 4.8 %. The capacity decreased to 312 mAh/g after 50 cycles for the cell with a carbon content of 49%. However, the uncoated silica reference cell displayed a capacity of 790 mAh/g after 50 cycles. This, and the potential profiles of the cells, suggests that the excessive SEI formation due to carbon coating hampers the silica conversion in the carbon coated cells, and that the carbon coating is detrimental to the performance of the cell. The difference in loading of the cells might also affect the performance, as the results are expected to be loading dependent due to the poor conductivity of silica.

The carbon coated cells displayed a significant initial capacity loss, which is expected for amorphous carbon. A capacity contribution from carbon was observed, but the carbon coating did not improve the capacity of the silica cells.

Despite the improved pyrolysis temperature of the carbon coating, the resulting capacities clearly revealed that the carbon coating of 4.8%-49% inhibit silica conversion of the cells. On the other hand, the pure silica cells are limited by low current densities due to their poor electrical conductivity leading to an IR loss. To improve the electrical and ionic conductivity in the electrode more research is needed.

Future work

To gain more insight into the obtained results, impedance measurements could be done on the active material, the thickness of the carbon layer could be measured with TEM, and the particle size of the silica particles could be measured.

In future work, the carbon coating can be done at sucrose concentrations between 5% and 20%, due to the significant capacity gap between the reference silica cell and the PMCC20 cell. Improvement in the carbon coating can be done by obtaining a lower surface area, which might decrease the SEI formation. A method for increasing conductivity that could be considered, is doping of the silica. This has been successful for silica nanoparticles [15].

Bibliography

[1] Svante Arrhenius. “On the Influence of Carbonic Acid in the Air upon the Temperature of the Ground”. In: *Philosophical Magazine and Journal of Science* 41 (1896), pp. 237–276.

[2] C.K. Folland et al. *Climate Change 2001: The Scientific Bases. Contribution of Working Group I to the Third Assessment Report of the Intergovernmental Panel on Climate Change*. Tech. rep. Cambridge, United Kingdom and New York, NY, USA: IPCC, 2001, p. 881.

[3] Terry L Root et al. “Fingerprints of global warming on wild animals and plants”. In: *Nature* 421.6918 (2003), pp. 57–60.

[4] Paul Denholm et al. *Overgeneration from Solar Energy in California. A Field Guide to the Duck Chart*. Tech. rep. Denver, CO, USA: National Renewable Energy Laboratory, 2015.

[5] EIA. *Levelized Cost and Levelized Avoided Cost of New Generation Resources in the Annual Energy Outlook 2018*. Tech. rep. U.S. Energy Information Administration, 2018, pp. 1–20.

[6] Yoshio Nishi. “The development of lithium ion secondary batteries”. In: *Chemical Records* 1.5 (2001), pp. 406–413.

[7] Thomas G Goonan. *Lithium Use in Batteries*. Tech. rep. Reston, Virginia, USA: U.S Geological Survey Circular 1371, 2012, p. 14.

[8] Qingsong Wang et al. “Environmental impact analysis and process optimization of batteries based on life cycle assessment”. In: *Journal of Cleaner Production* 174 (2018), pp. 1262–1273.

[9] Dominic A Notter et al. “Contribution of Li-Ion Batteries to the Environmental Impact of Electric Vehicles”. In: *Environmental science and technology* 44.17 (2010), pp. 6550–6556.

[10] Andrés Yaksic and John E Tilton. “Using the cumulative availability curve to assess the threat of mineral depletion : The case of lithium”. In: *Resources Policy* 34 (2009), pp. 185–194.

[11] Mats Zackrisson, Lars Avellán, and Jessica Orlenius. “Life cycle assessment of lithium-ion batteries for plug-in hybrid electric vehicles e Critical issues”. In: *Journal of Cleaner Production* 18.15 (2010), pp. 1519–1529.

[12] Christian Julien et al. *Lithium Batteries*. Springer, 2016.

[13] Qian Sun, Bing Zhang, and Zheng Wen Fu. “Lithium electrochemistry of SiO2 thin film electrode for lithium-ion batteries”. In: *Applied Surface Science* 254.13 (2008), pp. 3774–3779.

[14] Bingkun Guo et al. “Electrochemical reduction of nano-SiO2 in hard carbon as anode material for lithium ion batteries”. In: *Electrochemistry Communications* 10.12 (2008), pp. 1876–1878.

[15] Mingyuan Ge et al. “Scalable preparation of porous silicon nanoparticles and their application for lithium-ion battery anodes”. In: *Nano research* 6.3 (2013), pp. 174–181.

[16] *Silica*. 2018. URL: http://academic.eb.com/levels/collegiate/article/67757.

[17] Bo Gao et al. “Alloy formation in nanostructured silicon”. In: *Advanced Materials* 13.11 (2001), pp. 816–819.

[18] Won-Seok Chang et al. “Quartz (SiO2): a new energy storage anode material for Li-ion batteries”. In: *Energy & Environmental Science* 5.5 (2012), p. 6895.

[19] Anna Lisowska-Oleksiak, Andrzej P. Nowak, and Beata Wicikowska. “Aquatic biomass containing porous silica as an anode for lithium ion batteries”. In: *RSC Adv.* 4.76 (2014), pp. 40439–40443.

[20] By Manfred Sumper and Eike Brunner. “Learning from Diatoms : Nature ’ s Tools for the Production of Nanostructured Silica **”. In: *Advanced Functional Materials* 16.1 (2006), pp. 17–26.

[21] Clayton Jeffryes et al. “The potential of diatom nanobiotechnology for applications in solar cells , batteries , and electroluminescent devices”. In: *Energy & Environmental Science* 4 (2011), pp. 3930–3941.

[22] Victor Smetacek. “Diatoms and the Ocean Carbon Cycle”. In: *Protist* 150.1 (1999), pp. 25–32.

[23] Hua-Chao Tao et al. “Interweaved Si@SiOx/C nanoporous spheres as anode materials for Li-ion batteries”. In: *Solid State Ionics* 220 (2012), pp. 1–6.

[24] Mingqi Li et al. “Nanosilica/carbon composite spheres as anodes in Li-ion batteries with excellent cycle stability”. In: *J. Mater. Chem. A* 3.4 (2015), pp. 1476–1482.

[25] Yu Yao et al. “Carbon-coated SiO2 nanoparticles as anode material for lithium ion batteries”. In: *Journal of Power Sources* 196.23 (2011), pp. 10240–10243.

[26] M Ge et al. “Review of porous silicon preparation and its application for lithium-ion battery anodes”. In: *Nanotechnology* 24.42 (2013).

[27] Lars-Henrik Nysteen. “Exploring lithium ion batteries for wind powered water injection”. In: June (2016).

[28] Andreas Norberg. “SiO2 from Diatom Frustules as a High Performance, Low Cost and Environmentally Friendly Anode Material for Lithium Ion Batteries”. In: June (2017).

[29] A. Volta. *Del modo di rendere sensibilissima la più debole eletricità sia naturale, sia artificiale. Of the method of rendering very sensible the weakest natural or artificial Electricity*. 1782. URL: https://books.google.no/books?id=BDZWAAAAcAAJ.

[30] Antonia V Herzog, Timothy E Lipman, and Daniel M Kammen. *Renewable energy sources*. Tech. rep. Berkeley, USA: University of Cariformia, Berkeley, 2018, pp. 1–63.

[31] Bruno Scrosati. *Lithium batteries : advanced technologies and applications*. eng. Hoboken, NJ, 2013.

[32] Gilbert N. Lewis and Frederick G. Keyes. "The potential of the lithium electrode". In: *Journal of the American Chemical Society* 35.4 (1913), pp. 340–344.

[33] William Sidney Harris. "Electrochemical studies in cyclic esters". PhD thesis. University of California, 1958.

[34] J. B. Goodenough. *Electrochemical cell with new fast ion conductors*. 1981.

[35] K. Mizushima et al. "LixCoO2 (0¡x1): A new cathode material for batteries of high energy density". In: *Solid State Ionics* 3-4.C (1981), pp. 171–174.

[36] John B. Goodenough and Kyu Sung Park. "The Li-ion rechargeable battery: A perspective". In: *Journal of the American Chemical Society* 135.4 (2013), pp. 1167–1176.

[37] Keith B Oldham, Jan C Myland, and Alan M Bond. "Electrode Polarization". In: *Electrochemical Science and Technology: Fundamentals and Applications*. 1st ed. John Wiley & Sons, Ldt, 2012, pp. 193–212.

[38] Thomas Petry, Peter Schmid, and Christian Schlatter. "The use of toxic equivalency factors in assessing occupational and environmental health risk associated with exposure to airborne mixtures of polycyclic aromatic hydrocarbons (PAHs)". In: *Chemosphere* 32.4 (1996), pp. 639–648.

[39] Jian Guo Ren et al. "Germanium-graphene composite anode for high-energy lithium batteries with long cycle life". In: *Journal of Materials Chemistry A* 1.5 (2013), pp. 1821–1826.

[40] Yoshio Masaki, Akiya Kozawa, and Ralph J. Brodd. *Lithium-Ion Batteries*. Springer, 2013.

[41] Byoungwoo Kang and Gerbrand Ceder. "Battery materials for ultrafast charging and discharging". In: *Nature* 458.7235 (2009), pp. 190–193.

[42] Chunyan Lai et al. "Improved electrochemical performance of LiFePO4/C for lithium-ion batteries with two kinds of carbon sources". In: *Solid State Ionics* 179.27-32 (2008), pp. 1736–1739.

[43] Alexandre Magasinski et al. "Toward efficient binders for Li-ion battery Si-based anodes: Polyacrylic acid". In: *ACS Applied Materials and Interfaces* 2.11 (2010), pp. 3004–3010.

[44] Igor Kovalenko et al. "A Major Constituent of Brown Algae for". In: *Science* 334.6052 (2011), pp. 75–79.

[45] Pallavi Verma, Pascal Maire, and Petr Novák. "A review of the features and analyses of the solid electrolyte interphase in Li-ion batteries". In: *Electrochimica Acta* 55.22 (2010), pp. 6332–6341.

[46] S. S. Zhang, K. Xu, and T. R. Jow. "EIS study on the formation of solid electrolyte interface in Li-ion battery". In: *Electrochimica Acta* 51.8-9 (2006), pp. 1636–1640.

[47] Wei-Ming Zhang et al. "Carbon Coated Fe_3O_4 Nanospindles as a Superior Anode Material for Lithium-Ion Batteries". In: *Advanced Functional Materials* 18.24 (2008), pp. 3941–3946.

[48] Xiuwan Li et al. “Germanium anode with excellent lithium storage performance in a germanium/lithium-cobalt oxide lithium-ion battery”. In: *ACS Nano* 9.2 (2015), pp. 1858–1867.

[49] Kuok Hau Seng et al. “Self-assembled germanium/carbon nanostructures as high-power anode material for the lithium-ion battery”. In: *Angewandte Chemie - International Edition* 51.23 (2012), pp. 5657–5661.

[50] Meng He et al. “Monodisperse antimony nanocrystals for high-rate li-ion and na-ion battery anodes: Nano versus bulk”. In: *Nano Letters* 14.3 (2014), pp. 1255–1262.

[51] Yoshio Idota, Tadahiko Kubota, and Akihiro Matsufuji. “Tin-Based Amorphous Oxide : A High-Capacity Lithium-Ion – Storage Material”. In: *Science (New York, N.Y.)* 276.May (1997), p. 1395.

[52] Sangjin Han et al. “Simple synthesis of hollow tin dioxide microspheres and their application to lithium-ion battery anodes”. In: *Advanced Functional Materials* 15.11 (2005), pp. 1845–1850.

[53] Michael M. Thackeray et al. “Advances in manganese-oxide ’composite’ electrodes for lithium-ion batteries”. In: *Journal of Materials Chemistry* 15.23 (2005), pp. 2257–2267.

[54] W. Y. Li, L. N. Xu, and J. Chen. “Co3O4 Nanomaterials in Lithium-Ion Batteries and Gas Sensors”. In: *Advanced Functional Materials* 15.5 (2005), pp. 851–857.

[55] Bonil Koo et al. “Hollow iron oxide nanoparticles for application in lithium ion batteries”. In: *Nano Letters* 12.5 (2012), pp. 2429–2435.

[56] Qianjun He et al. “A novel mesoporous carbon@silicon–silica nanostructure for high-performance Li-ion battery anodes”. In: *Chem. Commun.* 50.90 (2014), pp. 13944–13947.

[57] J. Yang et al. “SiOx-based anodes for secondary lithium batteries”. In: *Solid State Ionics* 152-153 (2002), pp. 125–129.

[58] Manickam Sasidharan et al. “Synthesis, characterization and application for lithium-ion rechargeable batteries of hollow silica nanospheres”. In: *Journal of Materials Chemistry* 21.36 (2011), p. 13881.

[59] Nan Yan et al. “Hollow Porous SiO2 Nanocubes Towards High-performance Anodes for Lithium-ion Batteries”. In: *Scientific Reports* 3.1 (2013), p. 1568.

[60] Miran Gaberscek, Robert Dominko, and Janez Jamnik. “Is small particle size more important than carbon coating? An example study on $LiFePO_4$cathodes”. In: *Electrochemistry Communications* 9.12 (2007), pp. 2778–2783.

[61] Robert Kostecki et al. “Surface studies of carbon films from pyrolyzed photoresist”. In: *Thin Solid Films* 396.1-2 (2001), pp. 36–43.

[62] J. Coombs et al. “Studies on the biochemistry and fine structure of silica shell formation in diatoms. Photosynthesis and respiration in silicon-starvation synchrony of Navicula pelliculosa.” In: *Plant physiology* 42 (1967), pp. 1607–1611.

[63] T. Fuhrmann et al. “Diatoms as living photonic crystals”. In: *Applied Physics B: Lasers and Optics* 78.3-4 (2004), pp. 257–260.

[64] Stefano Lettieri et al. “The gas-detection properties of light-emitting diatoms”. In: *Advanced Functional Materials* 18.8 (2008), pp. 1257–1264.

[65] Soundarrajan Chandrasekaran et al. “Silicon diatom frustules as nanostructured photoelectrodes”. In: *Chemical Communications* 50.72 (2014), pp. 10441–10444.

[66] Clayton Jeffryes et al. “Electroluminescence and photoluminescence from nanostructured diatom frustules containing metabolically inserted germanium”. In: *Advanced Materials* 20.13 (2008), pp. 2633–2637.

[67] Luca De Stefano et al. “Lensless light focusing with the centric marine diatom Coscinodiscus walesii”. In: *Optics Express* 15.26 (2007), p. 18082.

[68] Richard L McCreery. *Raman spectroscopy for chemical analysis*. eng. New York, 2000.

[69] R Baddour-Hadjean and J P Pereira-Ramos. “Raman microspectrometry applied to the study of electrode materials for lithium batteries”. In: *Chemical Reviews* 110.3 (2010), pp. 1278–1319.

[70] J. Schwan et al. “Raman spectroscopy on amorphous carbon films”. In: *Journal of Applied Physics* 80.1 (1996), pp. 440–447.

[71] C Kittel. *Introduction to solid state physics. Fifth edition*. Jan. 1976.

[72] A. Broido. “A simple, sensitive graphical method of treating thermogravimetric analysis data”. In: *Journal of Polymer Science Part A-2: Polymer Physics* 7.10 (1969), pp. 1761–1773.

[73] Stephen Brunauer, P. H. Emmett, and Edward Teller. “Adsorption of Gases in Multimolecular Layers”. In: *Journal of the American Chemical Society* 60.2 (1938), pp. 309–319.

[74] Elliott P. Barrett, Leslie G. Joyner, and Paul P. Halenda. “The Determination of Pore Volume and Area Distributions in Porous Substances. I. Computations from Nitrogen Isotherms”. In: *Journal of the American Chemical Society* 73.1 (1951), pp. 373–380.

[75] Tao Zheng et al. “Lithium Insertion in High Capacity Carbonaceous Materials”. In: *Journal of the electrochemical sociely* 142.8 (1995).

[76] K Ogata et al. “Revealing lithium-silicide phase transformations in nano-structured silicon-based lithium ion batteries via in situ NMR spectroscopy”. In: *Nature Communications* 5.3217 (2014), pp. 1–11.